ELSEVIER

Chemical Engineering Journal 133 (2007) 121–131

Chemical Engineering Journal

www.elsevier.com/locate/cej

Using molecular simulations for screening of zeolites for separation of CO_2/CH_4 mixtures

R. Krishna*, J.M. van Baten

Van't Hoff Institute for Molecular Sciences, University of Amsterdam, Nieuwe Achtergracht 166, 1018 WV Amsterdam, The Netherlands

Received 26 November 2006; received in revised form 11 February 2007; accepted 19 February 2007

Abstract

Using Grand Canonical Monte Carlo (GCMC) and molecular dynamics (MD) simulation techniques 12 different zeolites were screened to determine which one would yield the best membrane separation selectivity for separation of CO_2 and CH_4. The choice of the zeolite has a significant influence on both the sorption and diffusion selectivities. It was found that zeolites CHA and DDR, that have cages separated by narrow windows, yielded the best permeation selectivities.

Keywords: Zeolites; Monte Carlo; Molecular dynamics; CO_2 separation; Membrane permeation; Separation selectivity

1. Introduction

The separation of CO_2 from natural gas is an important problem. The natural gas stream is available at high pressures of a few megapascals, and can be considered to be primarily methane (CH_4). CO_2 is a longer, slender molecule; CH_4 is a more compact molecule with a slightly larger cross-section. Fig. 1 presents cartoons showing approximate molecular dimensions of CO_2, CH_4 and N_2; these dimensions were estimated using published force fields for molecule–molecule interactions [1–3]. The subtle differences in the molecular dimensions of the two molecules can be exploited by allowing them to adsorb, and subsequently diffuse, across zeolite membranes [4–6]. From a practical point of view it is advantageous to use a membrane separation process in which CH_4 is retained on the high pressure side and CO_2 permeates selectively across to the membrane. Let us define the permeation selectivity

$$\alpha_{\text{perm}} = \frac{N_1/N_2}{f_1/f_2} \tag{1}$$

In Eq. (1) N_1 and N_2 represent the steady-state fluxes of $CO_2(1)$ and $CH_4(2)$ crossing the membrane and f_1 and f_2 are the partial gas phase fugacities of the two species in the upstream compartment of the membrane. The flux of any species is related to its chemical potential gradient by the Maxwell–Stefan equations [7]

$$-\rho\frac{q_i}{RT}\nabla\mu_i = \sum_{\substack{j=1\\ j\neq i}}^{n}\frac{q_jN_i - q_iN_j}{q_{j,\text{sat}}Đ_{ij}} + \frac{N_i}{Đ_i}, \quad i = 1,\ldots,n \tag{2}$$

In Eq. (2) $Đ_i$ is the Maxwell–Stefan diffusivity of species i, q_i the molar loading, $q_{i,\text{sat}}$ the saturation capacity of species i, and $Đ_{ij}$ are the binary exchange coefficients. The gradient of the chemical potentials can be related to the gradients in the loadings by defining a matrix of thermodynamic factors

$$\frac{q_i}{RT}\nabla\mu_i = \sum_{j=1}^{n}\Gamma_{ij}\nabla q_j, \quad \Gamma_{ij} \equiv \frac{q_i}{f_i}\frac{\partial f_i}{\partial q_j}, \quad i,j = 1,\ldots,n \tag{3}$$

The accurate determination of the saturation capacities $q_{i,\text{sat}}$ is essential in order to estimate the diffusion fluxes in the mixture; these can be obtained from the pure component sorption isotherms provided these are available up to saturation limits.

For *screening* purposes we consider an equimolar gas mixture in the upstream compartment, i.e. $f_1 = f_2$, take the downstream loadings to be vanishingly small, and approximate Eq. (4) by

$$\alpha_{\text{perm}} = \frac{D_{1,\text{self}}}{D_{2,\text{self}}}\frac{q_1}{q_2} = \alpha_{\text{diff}}\alpha_{\text{sorp}} \tag{4}$$

---

* Corresponding author. Tel.: +31 20 5257007; fax: +31 20 5255604.
E-mail address: r.krishna@uva.nl (R. Krishna).

1385-8947/$ – see front matter © 2007 Elsevier B.V. All rights reserved.
doi:10.1016/j.cej.2007.02.011

Nomenclature

Đ_i	Maxwell–Stefan diffusivity of species i ($m^2\,s^{-1}$)
f_i	fugacity of species i (Pa)
$\langle n_i \rangle$	ensemble average number of molecules in sampling volume
N_i	molar flux of species i across membrane ($mol\,m^{-2}\,s^{-1}$)
q_i	molar loading (mol/kg)
$q_{i,\mathrm{sat}}$	saturation loading (mol/kg)
R	gas constant (8.314 $J\,mol^{-1}\,K^{-1}$)
T	absolute temperature (K)

Greek letters

α_{diff}	diffusion selectivity
α_{perm}	permeation selectivity
α_{sorp}	sorption selectivity
Γ_{ij}	thermodynamic factors
θ_i	fractional occupancy of component i
μ_i	molar chemical potential ($J\,mol^{-1}$)
ρ	density of zeolite ($kg\,m^{-3}$)

Subscript

sat	referring to saturation conditions

where the diffusion selectivity α_{diff} is the ratio of the self-diffusivities of components 1 and 2, i.e.

$$\alpha_{\mathrm{diff}} = \frac{D_{1,\mathrm{self}}}{D_{2,\mathrm{self}}} \tag{5}$$

and the sorption selectivity α_{sorp} is defined as the ratio of the molar loadings q_i of CO_2 and CH_4 at the upstream face of the membrane

$$\alpha_{\mathrm{sorp}} = \frac{q_1}{q_2} \tag{6}$$

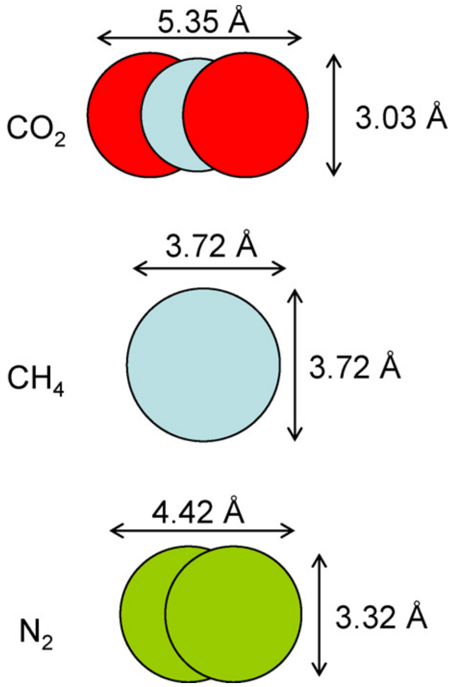

Fig. 1. Cartoon showing the approximate molecular dimensions of CO_2, CH_4 and N_2.

Recent development in Monte Carlo (MC) and molecular dynamics (MD) simulation techniques, coupled with the availability of high performance computing facilities, have enabled the determination of the adsorption and diffusion characteristics of a variety of molecules in different zeolites with a reasonable degree of accuracy and reliability [8–12]. An earlier study showed the utility of molecular simulations in screening zeolites for separation of hexane isomers [13]. The major objective of the current study is to illustrate the potential of MC and MD simulations in screening zeolites for separation of CH_4 and CO_2 for maximum permeation selectivity. We evaluate various zeolites in with regard to α_{sorp} and, subsequently, α_{diff}. We demonstrate that molecular simulations can provide insights into adsorption mechanisms, siting, orientation, and transport of molecules that are not available from experiments alone. Such insights allow the development of more fundamental models for process design.

2. Simulation results and discussion

More than 180 zeolite structures are known [14]. Fig. 2 shows some common topologies. The adsorption isotherms for pure CO_2, pure CH_4 and equimolar binary mixtures of CO_2 and CH_4 at 300 K in 12 different zeolites were computed using the Grand Canonical Monte Carlo (GCMC) technique. The chosen zeolites fall into three categories consisting of (a) one-dimensional channel structures (AFI, MOR, TON, FER, LTL), (b) intersecting channels (MFI, ISV, BEA), and (c) cages separated by windows (FAU, LTA, CHA, DDR). The simulation methodology, including a description of the force field, is given in Supplementary Data, that includes the complete set of information on the adsorption isotherms, along with snapshots showing the location of the molecules in the various zeolite structures. A selection of the important results is presented and discussed below.

Consider the pure component sorption isotherms of CO_2 and CH_4 in MFI determined experimentally by Zhu et al. [6], Golden and Sircar [15] and Kishima et al. [16]; see Fig. 3a and b. As is conventional, the data are plotted on linear axes. Zhu et al. [6] fitted the data with a single site Langmuir model with saturation capacities of 2.97 and 2.69 mol/kg for CO_2 and CH_4, respectively. When the same experimental data set is plotted with a logarithmic scale for the pressure axis it becomes apparent that for the range of pressures used in the experiments saturation was not achieved; see Fig. 3c and d. Also plotted in Fig. 3c and d are the GCMC simulation results that can be carried out to pressures say of 10^{11} Pa that are not accessible experimentally. The GCMC simulations suggest saturation capacities of 5.8 and 4 mol/kg for CO_2 and CH_4, respectively. These values correspond to values determined assuming that the pore volume is filled with saturated liquid.

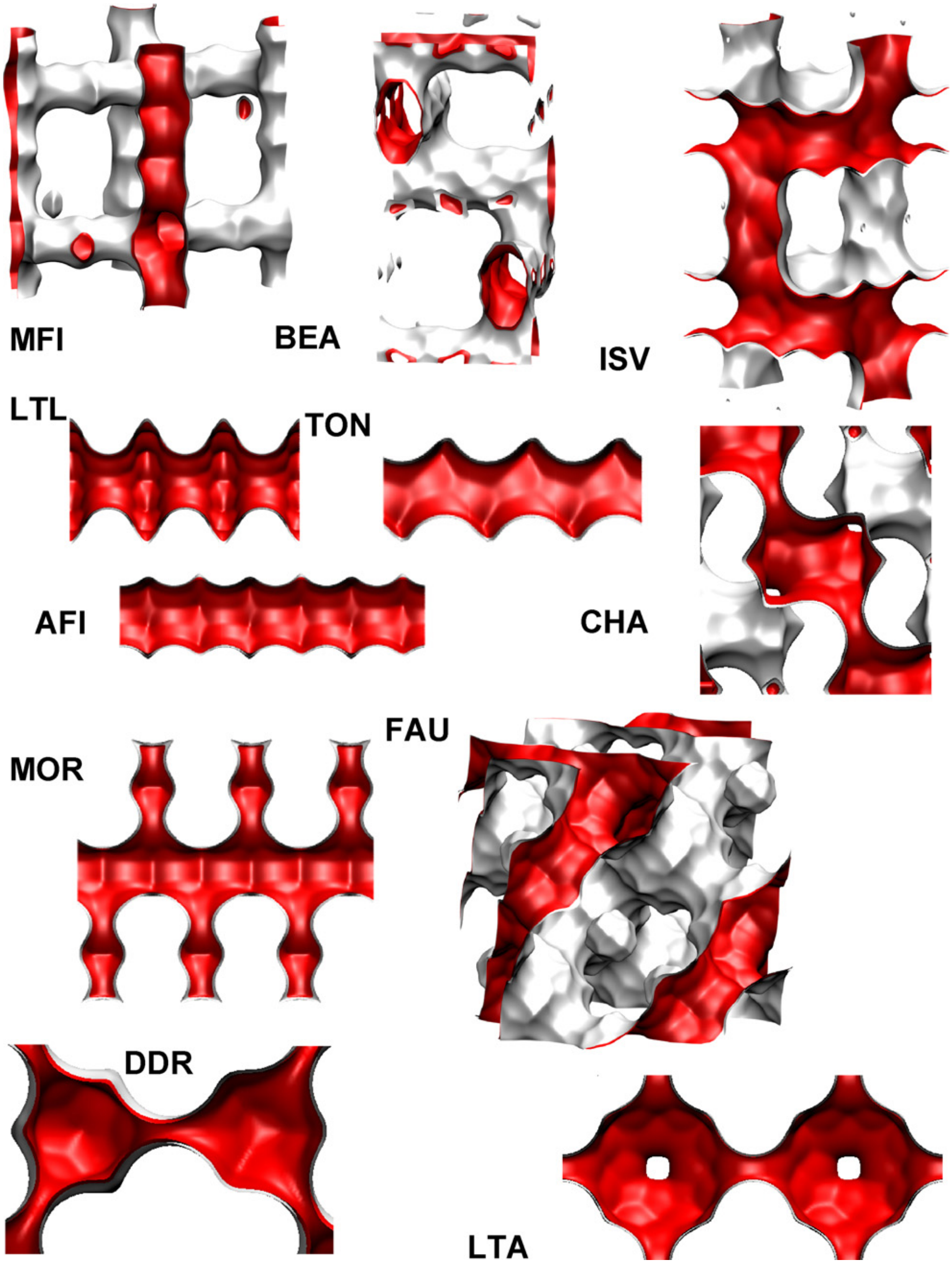

Fig. 2. A selection of zeolite structures. Note that the individual landscapes of zeolites are not all drawn to the same scale.

Fig. 4 shows the experimental data of Himeno et al. [17], indicated by the open symbols, for pure component isotherms of CO_2 and CH_4 in DDR for temperatures of (a) 273 K, (b) 298 K, (c) 323 K, and (d) 348 K. The filled symbols are GCMC simulation results; there is good agreement between the experiments and GCMC simulations confirming the correctness of the force field used in the simulations. On the basis of their experimental data Himeno et al. [17] obtained saturation capacities of approximately 2.8 and 1.7 mol/kg for CO_2 and CH_4, respectively. The GCMC simulation results appear to indicate that saturation was not achieved in the experiments and the true saturation capacities are significantly higher, about 4.6 and 4.2 mol/kg, for CO_2 and CH_4, respectively.

A further cautionary note is required when fitting of experimental isotherm data for CO_2 and CH_4. In almost all zeolites these molecules show inflection behavior and therefore a simple single site Langmuir fit is not justified. At least two-site, in most cases three-site Langmuir isotherm fits will be required [18]. This further underlines the problem of determining the saturation capacities from experimental isotherms an isotherm inflection can be mistaken to indicate saturation.

GCMC simulations for the component loadings in equilibrium with an equimolar gas mixture of CO_2 and CH_4 in (a) MFI, (b) CHA, and (c) DDR at 300 K are shown in Fig. 5. With increasing pressure the selectivity increases in favor of CO_2; the use of the multicomponent Langmuir model will yield selec-

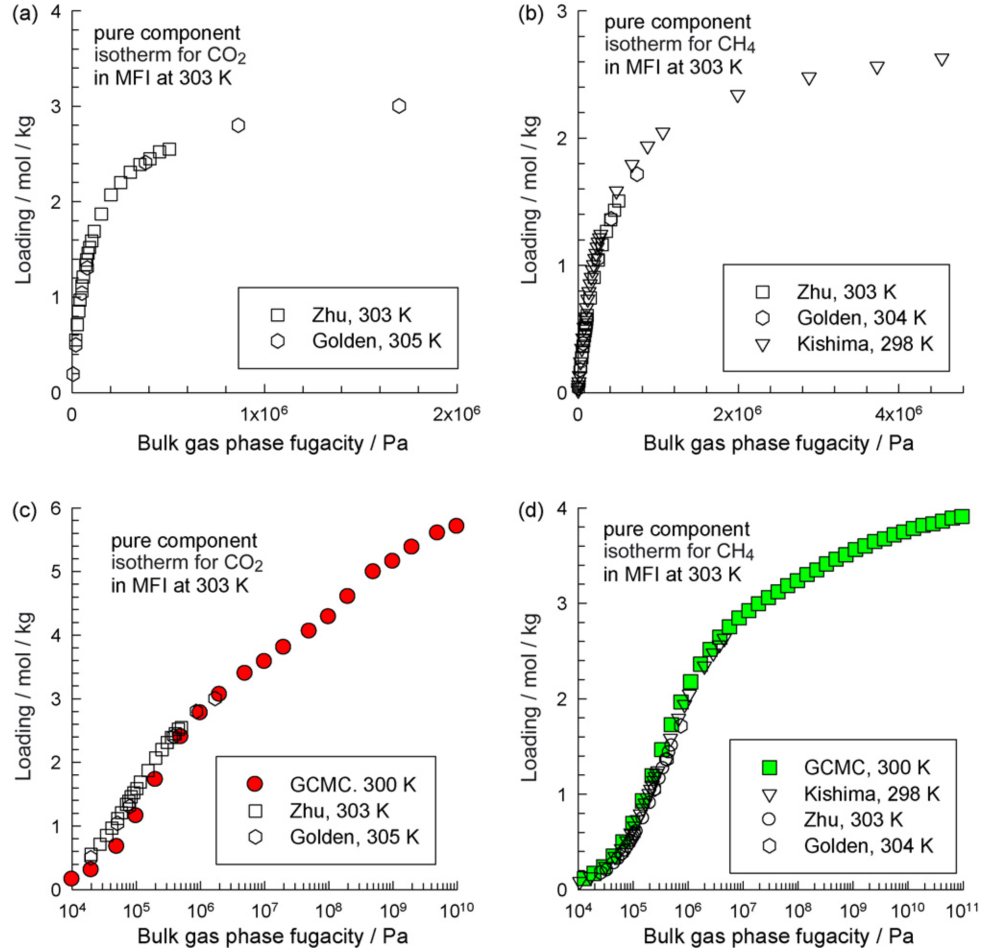

Fig. 3. Pure component sorption isotherm data for (a and c) CO_2 and (b and d) CH_4 in MFI at 298–305 K. The filled symbols are GCMC simulation results. The open symbols are experimental data of Zhu et al. [6], Golden and Sircar [15] and Kishima et al. [16].

tivities that are independent of the loadings and the pressure. Since the saturation capacities of CO_2 and CH_4 are significantly different from each other, the multicomponent Langmuir model cannot be used to calculate the component loadings for binary mixture sorption because of thermodynamic inconsistencies [19]. The continuous solid lines in Fig. 5 represent calculations of the IAST [20] using three-site Langmuir fits of pure component isotherms as given in an earlier publication [18]. The IAST provides a reasonable accurate estimation of loadings in the mixture and is recommended for use for process design.

The sorption selectivity $\alpha_{\text{sorp}} = q_1/q_2$ was determined from the component loadings for 12 different zeolites, divided into three categories: (a) uni-dimensional channels, (b) intersecting channels, and (c) cages-separated-by-windows; see Fig. 6. In all cases $\alpha_{\text{sorp}} = q_1/q_2$ increases with increasing values of $q = q_1 + q_2$. In order to verify that the separation selectivity hierarchy is not influenced by the presence of other species present in natural gas, such as N_2, simulations were also carried out for a mixture $CO_2/CH_4/N_2$; the results for $\alpha_{\text{sorp}} = q_1/q_2$ in this ternary mixture are presented in Fig. 7; the results show that the values of α_{sorp} are practically identical to the ones obtained in the binary mixture. On the basis of the simulation data on α_{sorp} we can narrow the choice of zeolite to MOR, LTL, MFI, CHA and DDR. We consider each of these zeolites in turn. We note that the α_{sorp} value for these zeolites are significantly higher than that of MWW, as reported in a recent molecular simulation study [21].

Let us first try to rationalize the α_{sorp} values observed for MOR at *low* loadings. For this purpose we examine the pure component sorption isotherms; see Fig. 8a. At pressures below about 20 kPa there is practically no adsorption of CH_4 while there is a finite adsorption of CO_2. The GCMC simulation results are in agreement with the experimental data (open symbols) of Delgado et al. [22] for H-MOR. A snapshot of CO_2 molecules within MOR at 300 K and $p = 10$ kPa is given in Fig. 8b; this shows that the CO_2 are exclusively located within the side pockets of MOR. Location within side pockets is not very effective during membrane permeation as the molecules cannot diffuse out, except via the main 12-ring channels. In order to confirm this we carried out MD simulations to determine self-diffusivities in an equimolar mixture of CO_2 and CH_4 in MOR at 300 K. The ratio of the self-diffusivities approximates α_{diff} and this data is presented in Fig. 8c. At low loadings the diffusivity of CO_2

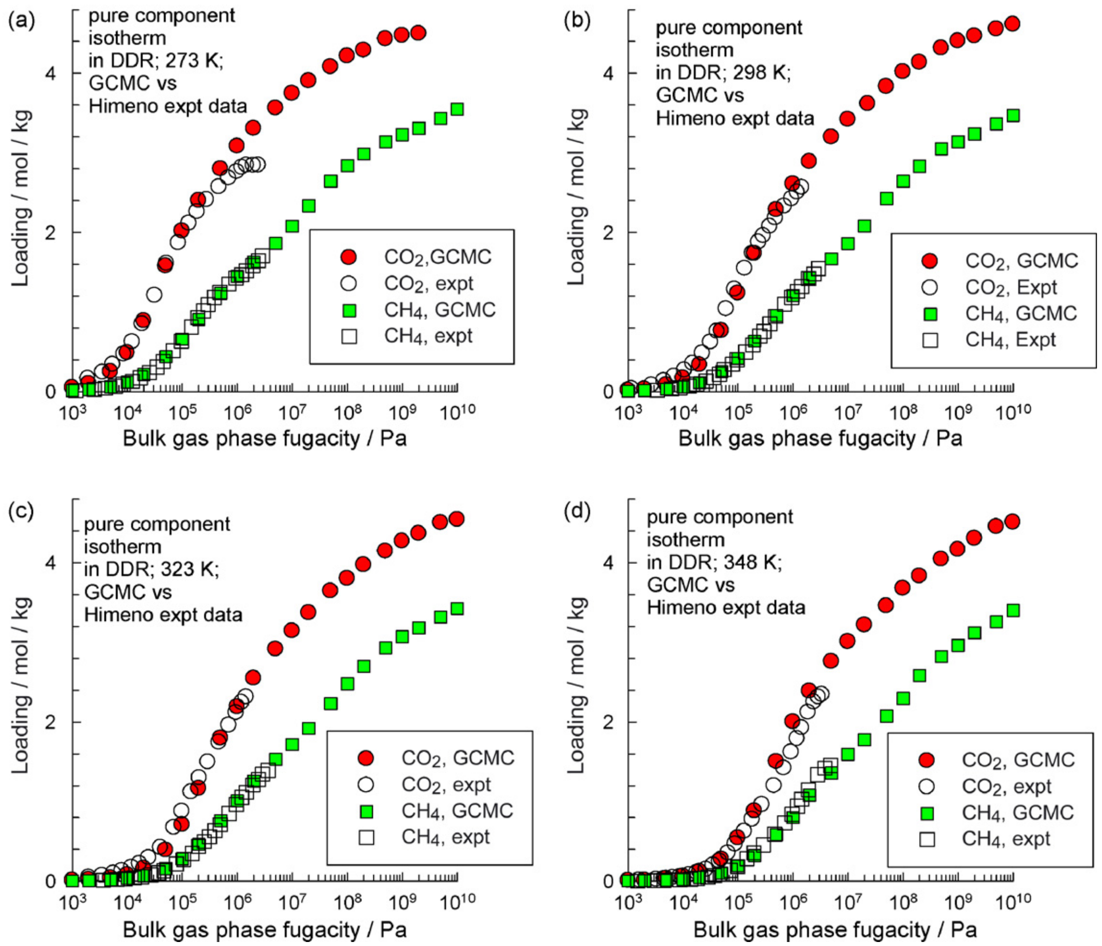

Fig. 4. Pure component sorption isotherm data for CO_2 and CH_4 in DDR at (a) 273 K, (b) 298 K, (c) 323 K, and (d) 348 K. The filled symbols are GCMC simulation results. The open symbols are experimental data of Himeno et al. [17] for DDR.

is about one order of magnitude lower than that of CH_4; this confirms the idea that at low loadings a vast majority of the CO_2 are trapped in the side pockets. Furthermore, we note that loadings in excess of 2 mol/kg the diffusivities of both species are practically the same. Molecular jumps in uni-dimensional channels are strongly correlated and both species have the same effective mobility; consequently $\alpha_{\mathrm{diff}} \approx 1$. An analogous picture holds for transport within the uni-dimensional channels of LTL; for this zeolite too the α_{diff} reach values of unity as the loading is increased above 2 mol/kg; see Fig. 8c. Let us turn to MFI which has an intersecting channel structure; see snapshot in Fig. 9a. Within the intersecting channels of MFI the molecular jumps of CO_2 and CH_4 are also strongly correlated [3] and therefore the values of α_{diff}, have values close to unity; cf. Fig. 8c.

The situation with respect to diffusion in CHA and DDR, both having cages separated by narrow windows, is different. Here the inter-cage hops of molecules through the narrow windows separating the two cages occur practically independently of one another because only one molecule can pass through a window at a given time [3]; see snapshots in Fig. 9b and c. CO_2 is a more slender molecule than CH_4, and the values of α_{diff} for CHA and DDR are significantly higher than unity; see Fig. 8c. The window size for DDR is smaller than that of CHA and this is the reason for its higher α_{diff}.

The differences in the mixture diffusion characteristics of various zeolite structures are also emphasized in earlier publications [23,24].

Fig. 10 summarizes the data on the permeation selectivity,α_{perm}, obtained as a product α_{sorp} and α_{diff}, as a function of total loading q for MFI, MOR, LTL, CHA and DDR zeolites. We see that the choice of ideal zeolite for use in membrane separations is between CHA and DDR. Also shown by filled symbols in Fig. 10 are experimental permeation selectivities as measured in DDR by van den Bergh et al. [25], and in SAPO-34, an isotype of CHA, by Li et al. [26,27]. The reasonably good agreement between the experimental permeation selectivities and calculations based on molecular simulations bear testimony to the accuracy and applicability of the approach followed in this paper. We also note that the permeation selectivities for CHA and DDR membranes are significantly higher than those obtained from FAU membranes with different Si/Al ratios [28].

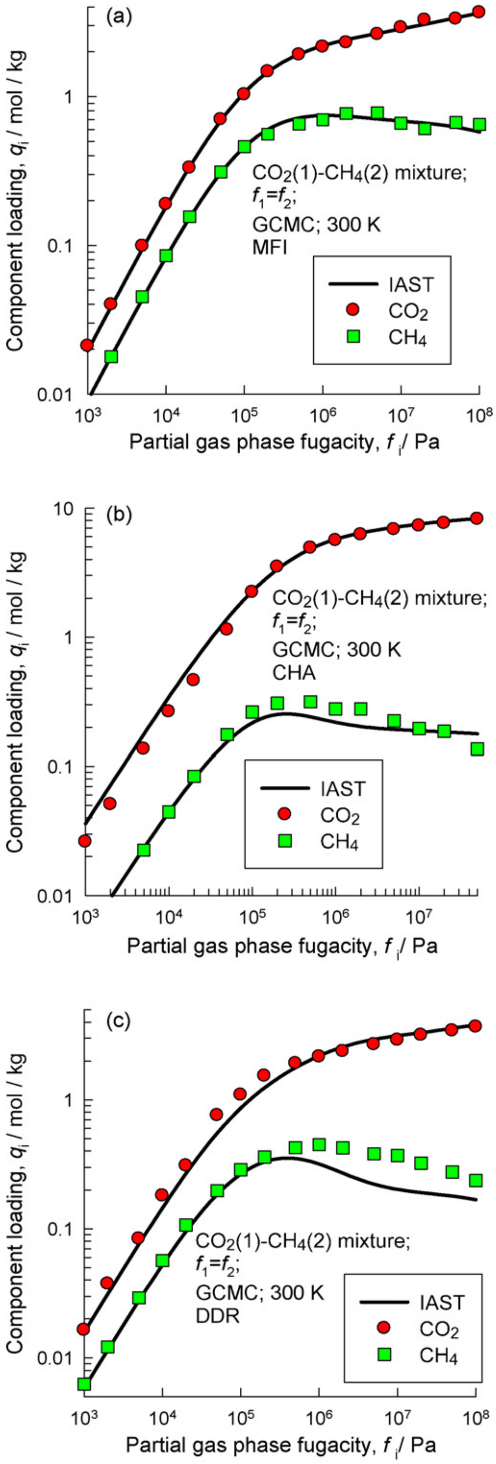

Fig. 5. GCMC simulations for the component loadings in equilibrium with an equimolar gas mixture of CO$_2$ and CH$_4$ in (a) MFI, (b) CHA, and (c) DDR at 300 K. The continuous solid lines represent calculations of the IAST [20] using three-site Langmuir fits of pure component isotherms; these fit parameters are given in Appendix A1 of the Supplementary Data accompanying this publication.

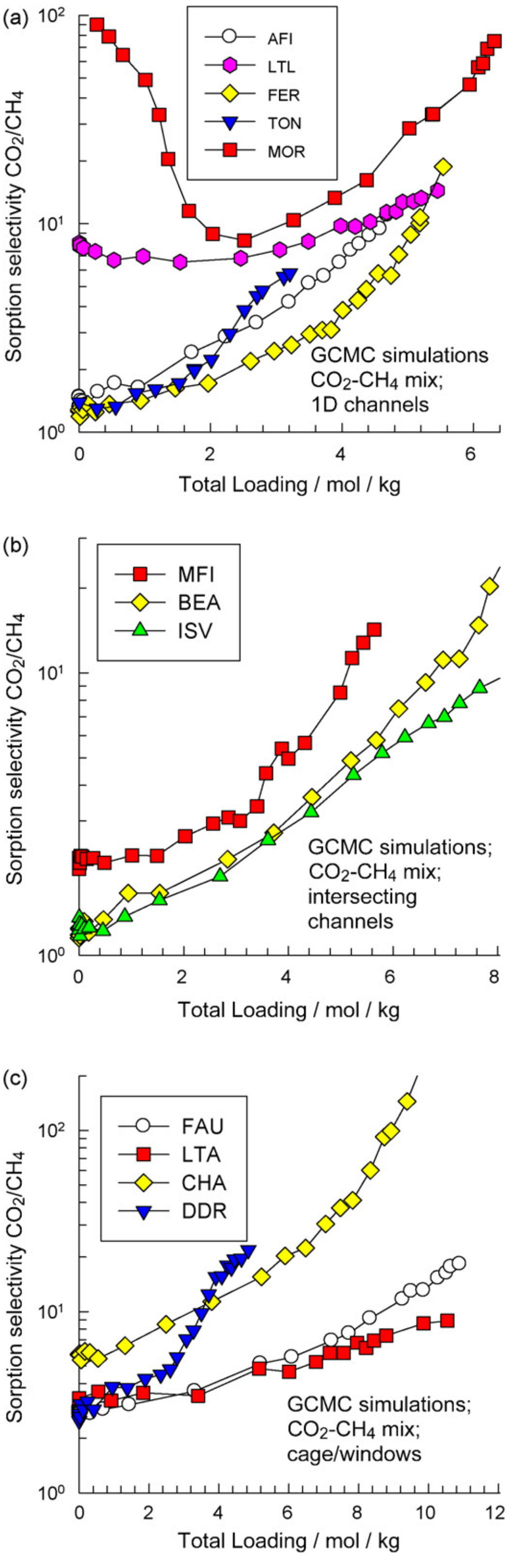

Fig. 6. CO$_2$/CH$_4$ sorption selectivity $\alpha_{\mathrm{sorp}} = q_1/q_2$ as a function of the total mixture loading $q = q_1 + q_2$, determined from GCMC binary mixture simulations, determined from GCMC simulations taking $f_1 = f_2$, for (a) one-dimensional channel structures (AFI, MOR, TON, FER, LTL), (b) intersecting channels (MFI, ISV, BEA), and (c) cages separated by windows (FAU, LTA, CHA, DDR).

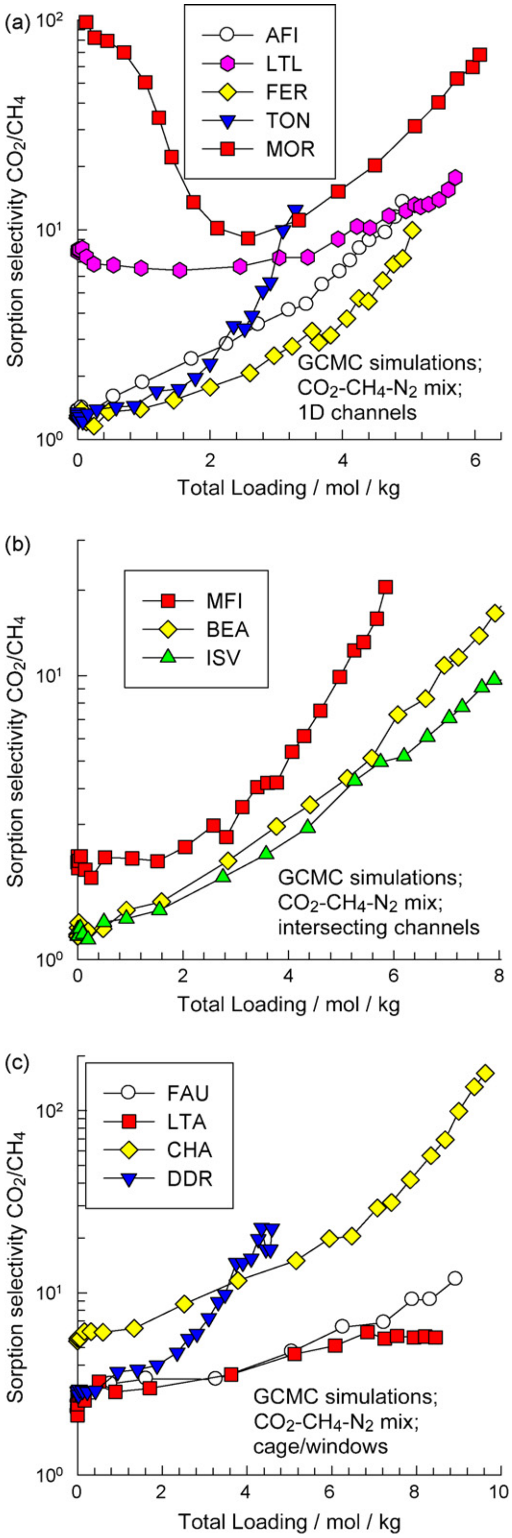

Fig. 7. CO_2/CH_4 sorption selectivity $\alpha_{\text{sorp}} = q_1/q_2$ as a function of the total mixture loading $q = q_1 + q_2 + q_3$ in ternary mixture $CO_2/CH_4/N_2$, determined from GCMC simulations taking $f_1 = f_2 = f_3$.

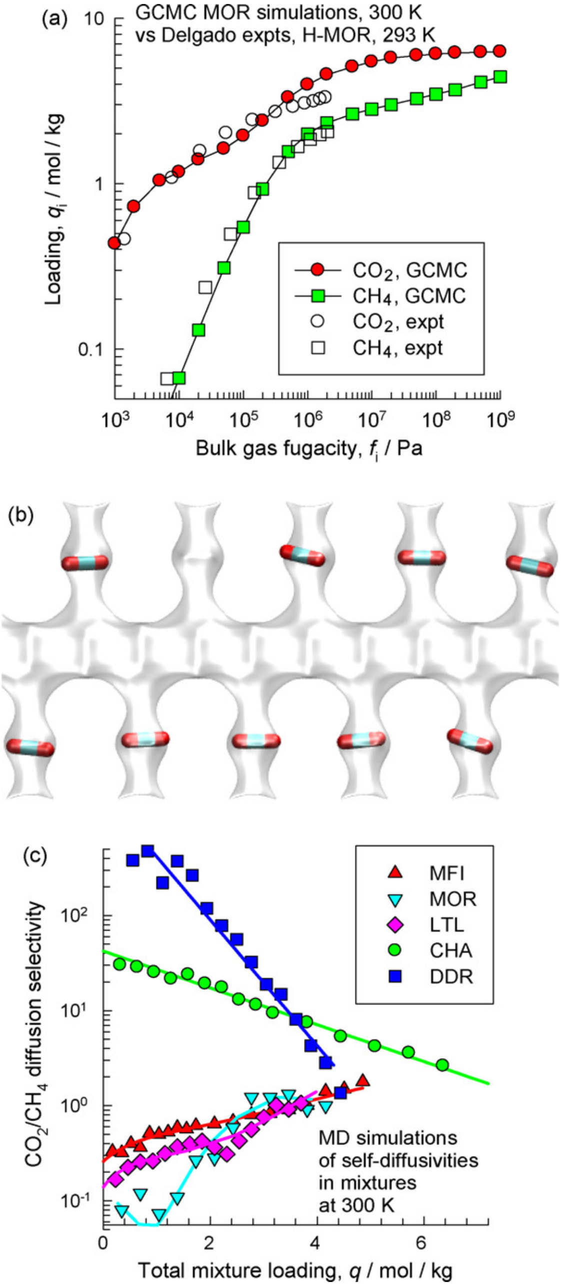

Fig. 8. (a) Pure component isotherm data for CO_2 and CH_4 in MOR at 300 K. Also shown are the experimental data (open symbols) of Delgado et al.[22] for H-MOR. (b) Snapshot of CO_2 in MOR at 300 K and $p = 10$ kPa. (c) The diffusion selectivity α_{diff} for various zeolites, calculated on the basis of MD simulations of self-diffusivities mixtures. The self-diffusivity data in for MFI, MOR and LTL are based on simulations of 1:1 mixtures of CO_2 and CH_4. For DDR and CHA the presented data are for 3:1 and 10:1 mixtures, respectively, in order to reflect the higher sorption selectivities for the zeolites.

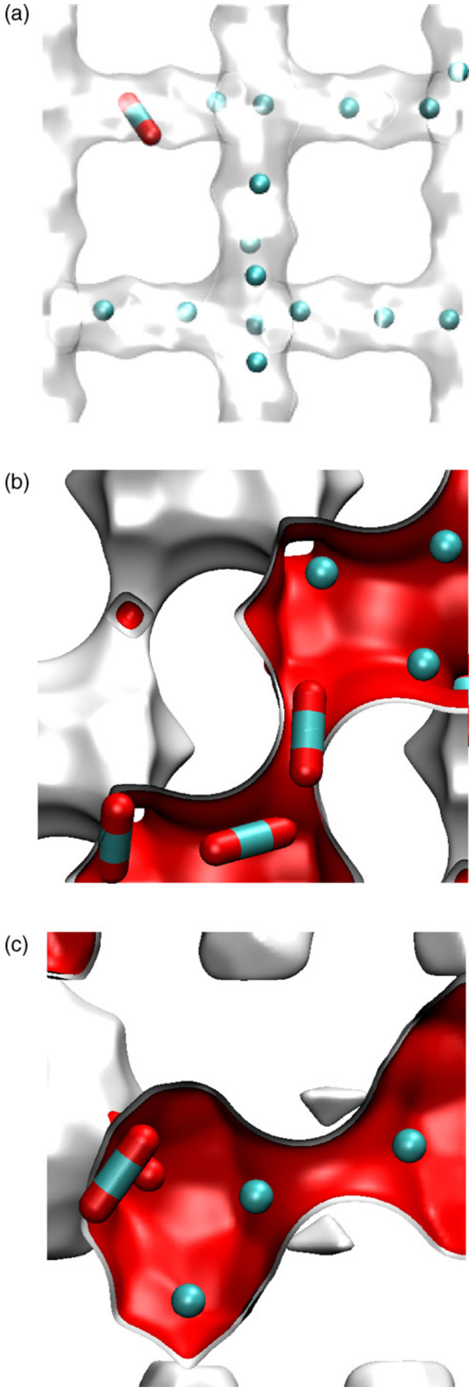

Fig. 9. Snapshots of CO_2 and CH_4 in (a) MFI, (b) CHA, and (c) DDR. These snapshots were made at partial fugacities of 500 and 9500 kPa, respectively for CO_2 and CH_4. Note that the individual snapshots are not all drawn to the same scale.

The permeation selectivity calculations using α_{perm} are good enough for screening purposes. For accurate process design calculations of the fluxes using the M-S equations we need the matrix of thermodynamic factor$[\Gamma]$ in Eq. (3). The fluctuation formula of Reed and Ehrlich [29] can be extended to a binary mixture to obtain the following expression for the *inverse* matrix of thermodynamic factors$[L]$:

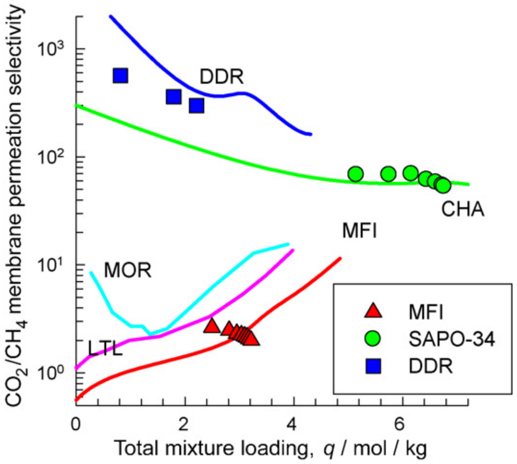

Fig. 10. The permeation selectivity, α_{perm} as a function of total loading q for MFI, MOR, LTL, CHA and DDR zeolites. Also shown by filled symbols are the experimental permeation selectivity data for DDR [25], and SAPO-34 [26,27].

$$L_{ji} \equiv \frac{f_i}{q_i}\frac{\partial q_j}{\partial f_i} = \frac{\langle n_i n_j\rangle - \langle n_i\rangle\langle n_j\rangle}{\langle n_i\rangle} \qquad (7)$$

The desired elements of the matrix of thermodynamic factors $[\Gamma]$ are obtained by matrix inversion:

$$[\Gamma] = [L]^{-1} \qquad (8)$$

GCMC simulations using Eq. (8) of $[\Gamma]$ for CO_2 (1)–CH_4 (2) mixtures in MFI, CHA, and DDR at 300 K are shown in Fig. 11. The continuous solid lines represent calculations of $[\Gamma]$ with IAST [20] using three-site Langmuir fits of pure component isotherms. It can be concluded that the IAST is of reasonable accuracy in process design calculations of the membrane permeation fluxes.

The procedure outlined above for screening of zeolites for CO_2/CH_4, separation can also be applied for separation of CO_2/N_2. Fig. 12 shows the CO_2/N_2 sorption selectivity,$\alpha_{\mathrm{sorp}} = q_1/q_3$, as a function of the total mixture loading $q = q_1 + q_2 + q_3$ in ternary mixture $CO_2/CH_4/N_2$, determined from GCMC simulations taking $f_1 = f_2 = f_3$. We conclude from this figure that the highest sorption selectivities are obtained with CHA zeolite. MD simulation results for self diffusivities in CO_2/N_2 mixtures in CHA are shown in Fig. 13a. We note that the diffusivity of CO_2 is smaller than that of N_2. Fig. 13b shows that the calculations of the α_{perm} for CHA compare reasonably well with the experimental data for Li et al. [26,27] for SAPO-34 membrane; the permeation selectivity values are in the range of 30–35, significantly higher than the values reported by Bernal et al. [30] for MFI membrane. We also note that our study contradicts the conclusions of Jia and Murad [31] who used MD simulations to conclude that the separation selectivity of CHA is lower than that of MFI and FAU.

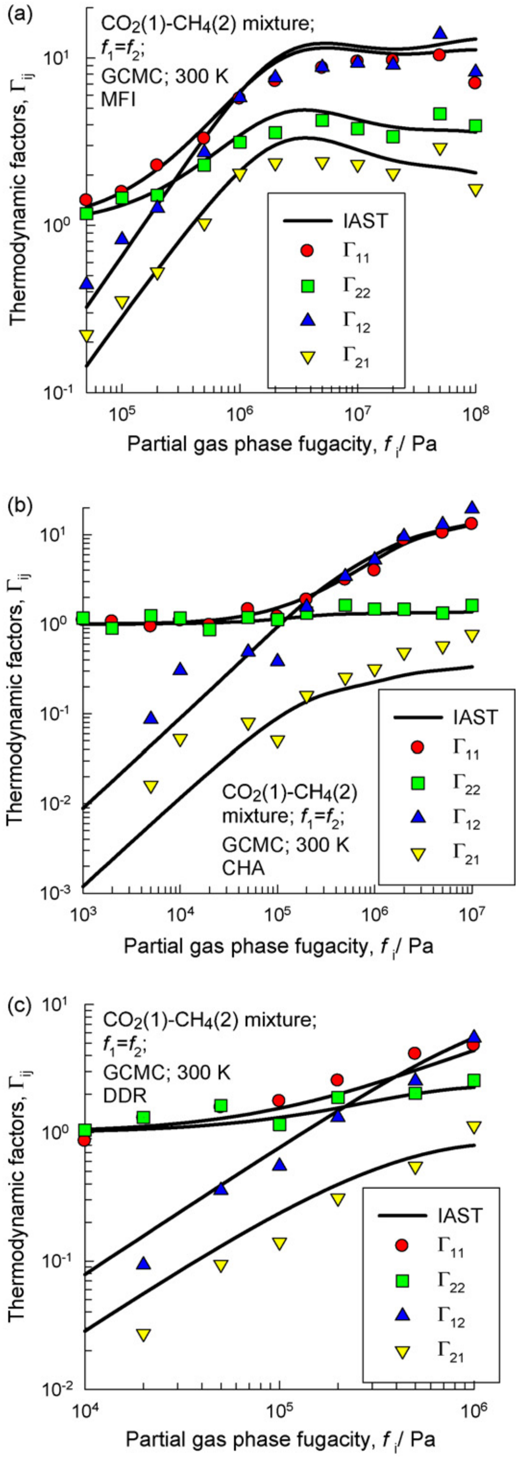

Fig. 11. GCMC simulations using Eq. (8) of [Γ] for $CO_2(1)$–$CH_4(2)$ mixtures in (a) MFI, (b) CHA, and (c) DDR at 300 K. The continuous solid lines represent calculations of [Γ] with IAST [20] using three-site Langmuir fits of pure component isotherms; these fit parameters are given in Appendix A1 of the Supplementary Data accompanying this publication.

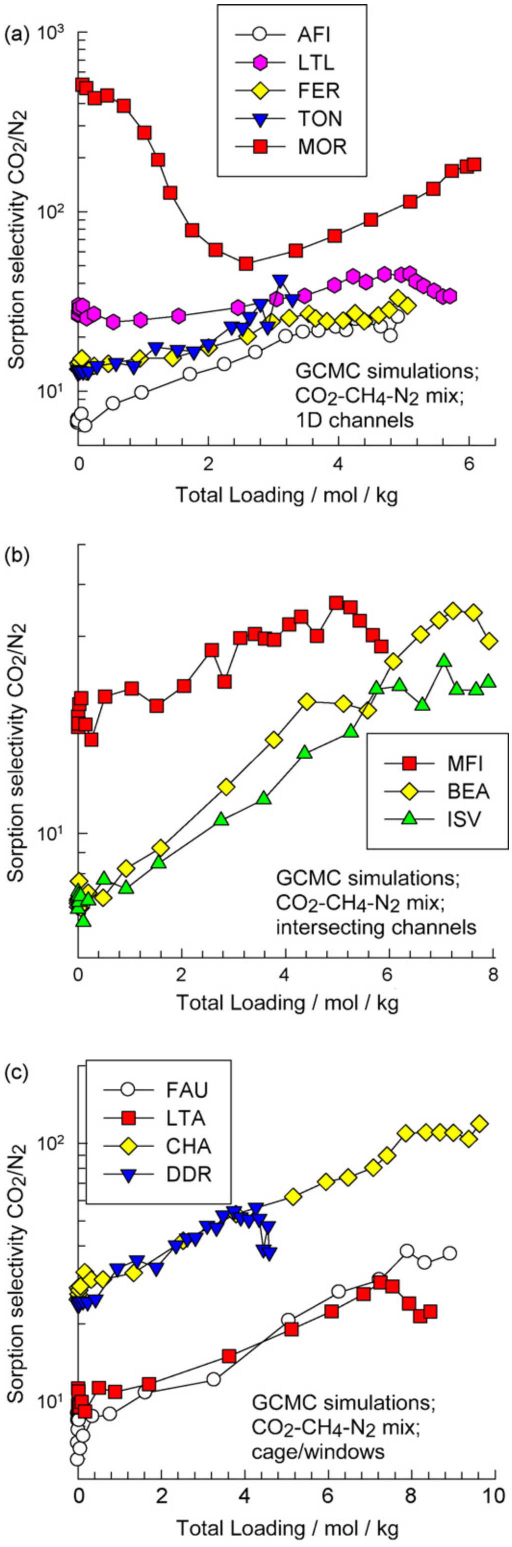

Fig. 12. CO_2/N_2 sorption selectivity $\alpha_{sorp} = q_1/q_3$ as a function of the total mixture loading $q = q_1 + q_2 + q_3$ in ternary mixture $CO_2/CH_4/N_2$, determined from GCMC simulations taking $f_1 = f_2 = f_3$.

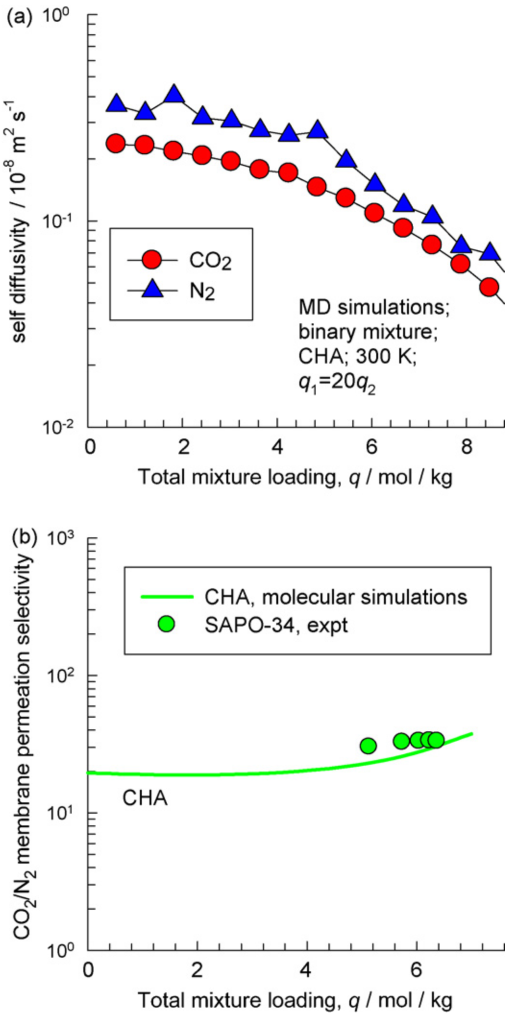

Fig. 13. (a) The CO_2/N_2 diffusion selectivity α_{diff} for CHA, calculated on the basis of MD simulations of self-diffusivities mixtures. The presented data are for 20:1 mixtures in order to reflect the higher sorption selectivities for the zeolites. (b) The CO_2/N_2 permeation selectivity, α_{perm} as a function of total loading q for CHA zeolite. Also shown by filled symbols are the experimental permeation selectivity data for SAPO-34 [26,27].

3. Conclusions

Twelve different zeolites were screened using GCMC and MD simulation to determine which one would lead to the best permeation selectivity α_{perm} in a membrane process for separation of CO_2 and CH_4. On the basis of sorption selectivities α_{sorp} the choice is narrowed to MOR, LTL, MFI, CHA and DDR. In one-dimensional channel structures (MOR, LTL) and in intersecting channel structures (MFI) there is strong correlation between the molecular jumps and therefore the diffusion selectivity α_{diff} is close to unity. High values of α_{diff} is achieved by choosing structures in which molecular jumps are uncorrelated; this is the case for zeolites, such as CHA and DDR, that consist of cages separated by narrow windows. CO_2 being a longer and slender molecule has a significantly higher diffusivity in such structures. Our study shows that highest α_{perm} is obtained using CHA and DDR. From a practical point of view other factors such as membrane permeation fluxes would also need to be considered in the final choice of zeolite membrane. Other considerations that impact on the choice of the zeolite membrane used include Si/Al ratio, membrane thickness, and characteristics of support layer.

Though the emphasis in this paper has been on screening of zeolites, molecular simulation data can also be used for process design and with continued advancement it may be reasonable to expect that processes can be developed and designed entirely *in silico*.

Acknowledgements

RK and JMvB acknowledge the grant of a TOP subsidy from The Netherlands Foundation for Fundamental Research (NWO-CW) for intensification of reactors and NWO/NCF for provision of high performance computing resources. The CBMC simulations were carried out with the BIGMAC program developed by Dr. T.J.H. Vlugt.

Appendix A. Supplementary data

Supplementary data associated with this article can be found, in the online version, at doi:10.1016/j.cej.2007.02.011.

References

[1] D. Dubbeldam, S. Calero, T.J.H. Vlugt, R. Krishna, T.L.M. Maesen, B. Smit, United atom forcefield for alkanes in nanoporous materials, J. Phys. Chem. B 108 (2004) 12301–12313.
[2] K. Makrodimitris, G.K. Papadopoulos, D.N. Theodorou, Prediction of permeation properties of CO_2 and N_2 through silicalite via molecular simulations, J. Phys. Chem. B 105 (2001) 777–788.
[3] R. Krishna, J.M. van Baten, E. García-Pérez, S. Calero, Diffusion of CH_4 and CO_2 in MFI, CHA and DDR zeolites, Chem. Phys. Lett. 429 (2006) 219–224.
[4] T. Tomita, K. Nakayama, H. Sakai, Gas separation characteristics of DDR type zeolite membrane, Micropor. Mesopor. Mater. 68 (2004) 71–75.
[5] S. Li, J.G. Martinek, J.L. Falconer, R.D. Noble, T.Q. Gardner, High-pressure CO_2/CH_4 separation using SAPO-34 membranes, Ind. Eng. Chem. Res. 44 (2005) 3220–3228.
[6] W. Zhu, P. Hrabanek, L. Gora, F. Kapteijn, J.A. Moulijn, Role of adsorption in the permeation of CH_4 and CO_2 through a silicalite-1 membrane, Ind. Eng. Chem. Res. 45 (2006) 767–776.
[7] R. Krishna, J.M. van Baten, Describing binary mixture diffusion in carbon nanotubes with the Maxwell–Stefan equations. An investigation using molecular dynamics simulations, Ind. Eng. Chem. Res. 45 (2006) 2084–2093.
[8] J. Kärger, S. Vasenkov, S.M. Auerbach, Diffusion in zeolites, in: S.M. Auerbach, K.A. Carrado, P.K. Dutta (Eds.), Handbook of Zeolite Science and Technology, Marcel Dekker, New York, 2003, pp. 341–422 (Chapter 10).
[9] D. Frenkel, B. Smit, Understanding Molecular Simulations: From Algorithms to Applications, 2nd ed., Academic Press, San Diego, 2002.
[10] A.H. Fuchs, A.K. Cheetham, Adsorption of guest molecules in zeolitic materials: computational aspects, J. Phys. Chem. B 105 (2001) 7375–7383.
[11] B. Smit, R. Krishna, Molecular simulations in zeolitic process design, Chem. Eng. Sci. 58 (2003) 557–568.
[12] R. Krishna, B. Smit, S. Calero, Entropy effects during sorption of alkanes in zeolites, Chem. Soc. Rev. 31 (2002) 185–194.
[13] R. Krishna, J.M. van Baten, Screening of zeolite adsorbents for separation of hexane isomers: a molecular simulation study, Sep. Purif. Technol. 55 (2007) 246–255, doi:10.1016/j.seppur.2006.12.01.

[14] C. Baerlocher, W.M. Meier, D.H. Olson, Atlas of Zeolite Framework Types, 5th ed., Elsevier, Amsterdam, 2002.

[15] T.C. Golden, S. Sircar, Gas-adsorption on silicalite, J. Coll. Interf. Sci. 162 (1994) 182–188.

[16] M. Kishima, H. Mizuhata, T. Okubo, Effects of confinement on the adsorption behavior of methane in high-silica zeolites, J. Phys. Chem. B 110 (2006) 13889–13896.

[17] S. Himeno, T. Tomita, K. Suzuki, S. Yoshida, Characterization and selectivity for methane and carbon dioxide adsorption on the all-silica DD3R zeolite, Micropor. Mesopor. Mater. 98 (2007) 62–69.

[18] R. Krishna, J.M. van Baten, E. García-Pérez, S. Calero, Incorporating the loading dependence of the Maxwell–Stefan diffusivity in the modeling of CH_4 and CO_2 permeation across zeolite membranes, Ind. Eng. Chem. Res. 46 (2007), doi:10.1021/ie060693d.

[19] M.B. Rao, S. Sircar, Thermodynamic consistency for binary gas adsorption equilibria, Langmuir 15 (1999) 7258–7267.

[20] A.L. Myers, J.M. Prausnitz, Thermodynamics of mixed gas adsorption, AIChE J. 11 (1965) 121–130.

[21] J.M. Leyssale, G.K. Papadopoulos, D.N. Theodorou, Sorption thermodynamics of CO_2, CH_4, and their mixtures in the ITQ-1 zeolite as revealed by molecular simulations, J. Phys. Chem. B 110 (2006) 22742–22753.

[22] J.A. Delgado, M.A. Uguina, J.M. Gómez, L. Ortega, Adsorption equilibrium of carbon dioxide, methane and nitrogen onto Na- and H-mordenite at high pressures, Sep. Purif. Technol. 48 (2006) 223–228.

[23] R. Krishna, J.M. van Baten, A molecular dynamics investigation of diffusion of methane–ethane and methane–propane mixtures in zeolites, Chem. Eng. Technol. 29 (2006) 1429–1437.

[24] R. Krishna, J.M. van Baten, Diffusion of alkane mixtures in MFI zeolite, Micropor. Mesopor. Mater. (2007), doi:10.1016/j.micromeso.2006.11.032.

[25] J. van den Bergh, W. Zhu, J.C. Groen, F. Kapteijn, J.A. Moulijn, K. Yajima, K. Nakayama, T. Tomita, S. Yoshida, Natural gas purification with a ddr zeolite membrane; permeation modelling with Maxwell–Stefan equations, in: Proceedings of the 15th International Zeolite Conference, Beijing, China, 2007.

[26] S. Li, J.L. Falconer, R.D. Noble, R. Krishna, Modelling permeation of CO_2/CH_4, CO_2/N_2, and N_2/CH_4 mixtures across SAPO-34 membrane with the Maxwell–Stefan equations, Ind. Eng. Chem. Res. 46 (2007), doi:10.1021/ie0610703.

[27] S. Li, J.L. Falconer, R.D. Noble, R. Krishna, Interpreting unary, binary and ternary mixture permeation across a SAPO-34 membrane with loading-dependent Maxwell–Stefan diffusivities, J. Phys. Chem. C 111 (2007), doi:10.1021/jp067404j.

[28] Y. Hasegawa, T. Tanaka, K. Watanabe, B.H. Jeong, K. Kusakabe, S. Morooka, Separation of CO_2–CH_4 and CO_2–N_2 systems using ion-exchanged FAU-type zeolite membranes with different Si/Al ratios, Kor. J. Chem. Eng. 19 (2002) 309–313.

[29] D.A. Reed, G. Ehrlich, Surface diffusion, atomic jump rates and thermodynamics, Surf. Sci. 102 (1981) 588–609.

[30] M.P. Bernal, J. Coronas, M. Menendez, J. Santamaria, Separation of CO_2/N_2 mixtures using MFI-type zeolite membranes, AIChE J. 50 (2004) 127–135.

[31] W. Jia, S. Murad, Separation of gas mixtures using a range of zeolite membranes: a molecular-dynamics study, J. Chem. Phys. 122 (2005) 234708.